Timing Offset and Timing Stability for a Dual-Clock Channel Sounder

Joshua M. Kast, Jacob D. Rezac, Stefania Römisch, Atef Z. Elsherbeni and Jeanne T. Quimby

Abstract—**We describe a mathematical framework for evaluating timing offset and timing noise in channel sounders based on a second-order deterministic model and a stochastic metric based on the Allan Deviation. Using this framework, we analyze the timing offset and noise for a 1-6 GHz correlation-based channel sounder that uses rubidium clocks to provide a common timebase between the transmitter and receiver. We study timing behavior in three clock-distribution configurations. In the "untethered" configuration, the transmitter and receiver each have a rubidium clock, and no physical timing cable is connected between the clocks. In the "tethered" configuration, a coaxial cable synchronizes timing between the two separate clocks. Finally, a benchmark "single-clock" configuration is used where a single rubidium clock drives the transmitter and receiver.**

Index Terms— **5G technology; channel sounder; millimeter-wave wireless communication; propagation channel; system timing, Time Allan Deviation; timing errors; timing noise; timing offset; wireless system.**

I. INTRODUCTION

FIFTH-GENERATION (5G) wireless devices rely heavily upon channel models to derive system specifications [1].

Effective data-driven channel models originate from the reliable evaluation of real-world channel propagation. Channel sounders and channel-sounding measurements are an important part of this evaluation. Part of the measurement best-practices is the verification of the channel sounder's hardware [2].

In this work, which builds upon the foundation set by [3], we quantify timing offset and timing stability in a 1-6 GHz correlation-based channel sounder. This is vital because channel sounding relies on high-quality time synchronization between a channel sounder's transmitter (Tx) and receiver (Rx). Metrology applications require a complete uncertainty analysis for channel sounders. Currently, this uncertainty analysis is incomplete because timing uncertainties are not included. This paper provides a novel approach by applying established timing models as a first step in the determination of complete uncertainty of a dual-clock channel sounder. It is important to note that while this paper uses the example of a dual-clock channel sounder, the methodology described here can be used for other systems with a dual-clock timing method.

Typical post-processing of channel-sounding data is based on the assumption that the Tx and Rx share a common time-base and frequency reference. However, all frequency standards are known to have non-idealities [5][6]. Initial synchronization offset, frequency offset, frequency drift, and stochastic noise are captured by the quantity termed here as "timing offset." There are various ways timing offset is manifested in channel sounders: for example, time offset due to the rubidium clocks, offset due to the timing circuitry of the Tx and Rx, and offset due to phase instabilities in coaxial cables. During our studies, we found significant differences in timing offset depending on the configuration of the rubidium (Rb) clocks in our systems.

In this paper we quantify the timing offset of a microwave correlation-based channel sounder that uses a pair of separate Rb clocks as frequency standards for the Tx and Rx [2]. The analysis presented here may also be applied to millimeter-wave channel sounders. We study the impact of three different timing configurations on time-synchronization and quantify the timing effects using deterministic and stochastic mathematical approaches [7].

The deterministic approach uses a second-order model which aims to capture the timing drift. The stochastic mathematical approach uses a statistical description of observed timing noise based on the Time Deviation, related to the Allan Deviation [8]. Understanding the results from these approaches may lead to design and/or hardware improvements in the channel sounder or similar systems, since potential sources of timing noise may be identified.

We define the following terms which will be used repeatedly below [7]:

Timing offset (x_i) – The time difference between two clocks. For this paper, this means the time difference between the Rb clocks in the Tx system and Rx system of the channel sounder.

Timing stability – The variability in timing offset due to noise processes.

Synchronization – Aligning Tx and Rx system events to occur at the same time.

Syntonization – Aligning Tx and Rx systems to operate at the same frequency [5]-[8].

A. Prior Work

Numerous channel sounders use rubidium (Rb) frequency reference "clocks" to achieve synchronization and syntonization between the Tx and Rx [4]. Rb clocks are integrated in many channel-sounder implementations described in the literature. However, such descriptions may not give
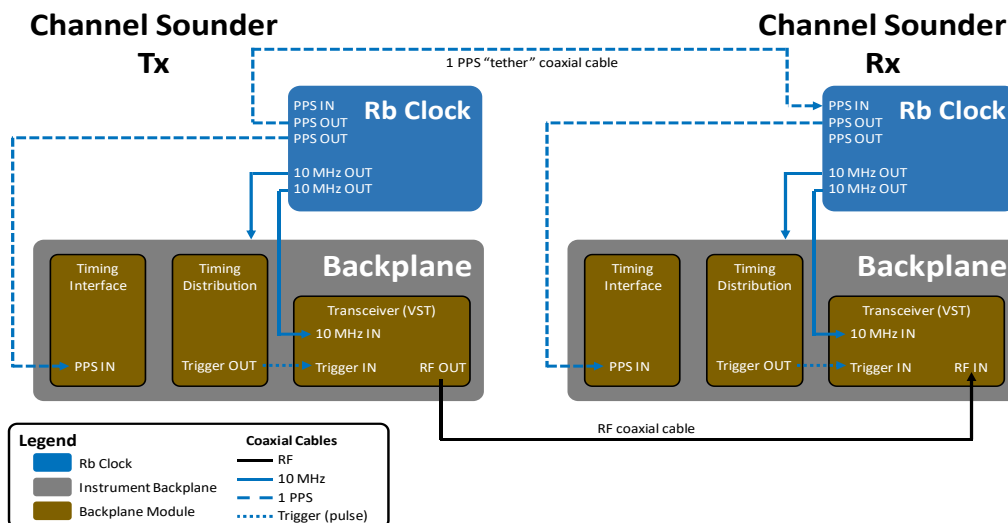
Fig. 1: Block diagram of the channel sounder used in this work, in the tethered configuration. Instrument backplanes contain modules for timing interface and distribution, as well as a vector signal transceiver. External Rb clocks supply modules within the Tx and Rx backplanes with 10 MHz and 1 PPS (pulse-per-second) timing signals. Additionally, the backplane accepts a 10 MHz signal from the Rb clock and distributes it to installed modules.

specific details on the clock setup, syntonization, or uncertainty [9]-[13].

In some work, Rb clocks are integrated into channel sounders, and the calibration or characterization of the Rb clocks is described directly [14]-[16]. Additionally, many systems rely on Rb clocks synchronized with GPS signals [17]-[24]. Synchronization via GPS is important for applications involving high-speed moving vehicles, where cable tethers are not practical, and GPS data may be utilized for both timing and position information [25].

Rb clock modules were stored in temperature-controlled enclosures, and system timing was measured at the start and end of each experiment to account for time drift [26]. In another work, a linear model was applied in [4] to correct for time drift. This work's approach compared system timing wirelessly using a known line-of-sight channel [27]. Additionally, millimeter-wave channel sounders with multiple-input multiple-output (MIMO) architecture require time-alignment of their multiple spatial channel measurements [28]. This research was interested in millimeter-wave applications and focused on channel-sounder measurement durations on the order of milliseconds. Building upon this work, we performed repeat channel-sounder measurements with a duration of multiple days. These measurements enabled a capture of the deterministic and stochastic timing quantities over a superset of time scales.

In one system, syntonization of frequency and initiation of Tx and Rx functions are carried out in two separate procedures [29]-[31]. In other systems, cesium clocks are used, which have a greater stability than Rb, but at a higher cost [32]-[34]. As frequencies increases in the channel sounder measurements, increased phase accuracies are required to mitigate systematic errors due to absolute phase deviation of the equipment.

Apart from channel sounding, numerous measurement applications require precise time alignment between instruments. Measurements of high-frequency signals impose increased requirements for time alignment. For example, in the work of [35], an indirect method for phase-error quantification and uncertainty analysis is reported for digitizers. Millimeter signal measurements, such as those used for RF applications, require increased phase stability. Commercial software-defined radio (SDR) equipment has been used to make phase measurements of both pulsed and sinusoidal time-reference signals [36].

A survey of the literature demonstrates that timing is often seen as an important characteristic of a channel-sounder design. In this work, we aim to complement the existing descriptions of channel sounder designs by demonstrating a systematic approach by which users of channel sounders may evaluate the timing stability of their own channel sounders and quantify the effects of any subsequent improvements they make. We provide a comprehensive set of measurements on multiple channel-sounder configurations, which designers may use to further understand the impact of architecture on channel-sounder timing stability.

II. CHANNEL SOUNDER TIMING CONFIGURATIONS

Our channel sounder used two high-stability Rb clocks to obtain a common time-base between the Tx and Rx, as seen in Fig. 1, Fig. 2 and Fig. 3. These Rb clocks serve as 10 MHz frequency references for the channel sounder's local oscillators (LO). Additionally, digital-to-analog and analog-to-digital circuits within the channel sounder use these clocks as a reference for their sampling rates.

We chose to compare three different configurations for our Rb clock-based system timing. In the benchmark "common-clock" configuration depicted in Fig. 2 (a), the Tx and Rx are connected to 10 MHz and 1 pulse per second (PPS) [37] outputs from the Rb clock. This configuration provides excellent synchronization but is not practical for long-distance measurements due to the need for coaxial timing connections between the Tx, Rx, and Rb clock.

Another common timing configuration [4] which we call "tethered" uses separate Rb clocks for the Tx and Rx that are connected by a single coaxial link as shown in Fig. 2 (b). The Rx Rb clock synchronizes its internal oscillator to the PPS signal carried over the coaxial cable.

We labeled the final timing configuration "untethered"
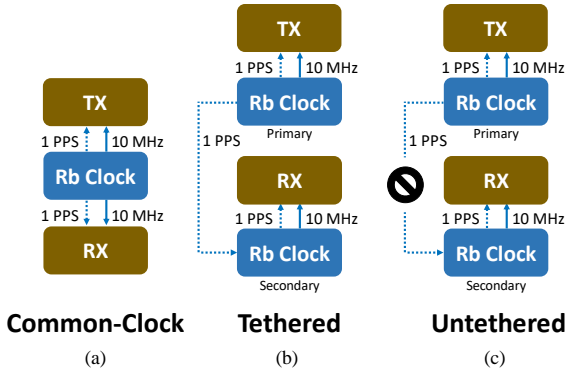
Fig. 2: Block diagram of the three channel sounder timing configurations used in this work: (a) common-clock, (b) tethered, and (c), untethered

Fig. 3: Channel sounder hardware used for timing experiments. From top to bottom: receiver unit, pair of Rb clocks, and transmitter unit. In this image, the cables for PPS and 10 MHz timing signals are visible, but power, RF, and computer cabling are removed for clarity.

because while there are still two separate clocks there is no physical cable connecting the Tx and Rx as seen in Fig. 2 (c). Channel-sounder measurements in an industrial environment necessitate an untethered Tx and Rx, because a cable crossing such an environment may present a trip hazard or be damaged by industrial machinery. Prior to measurements, we synchronized and thus also syntonized the clocks using a PPS signal carried over coaxial cable for 72 hours. In this study, we tested whether this 72-hour period was really needed. Equally, we were interested in learning about the amount of drift after we removed the PPS connection.

A. Rubidium Clocks and Oscillators

A clock has two components: an oscillator and a frequency divider. The oscillator supplies a signal with a well-defined frequency. The frequency-divider converts the oscillations to lower frequency pulses, which may occur at meaningful units of time such as seconds [38]. Advances in technology have improved the stability of oscillators, allowing modern clocks to maintain precise time over longer periods.

The rubidium clocks in this work use a closed-loop feedback mechanism where a 10 MHz quartz oscillator's frequency is adjusted based on the hyperfine transition frequency of the Rb atom [39]. The 1 PPS output is a result of the division of the oscillator's 10 MHz signal.

We use the Rb clocks in their capacity as oscillators, by supplying the 10 MHz signal to the Tx and Rx of our channel sounder, where it is used as a frequency reference for synthesis of the local-oscillator (LO) and analog-to-digital converter (ADC) sampling frequency. Additionally, we use the Rb clocks in their capacity as clocks, by using the 1 PPS signal as a phase-reference to synchronize RF transmission by the Tx, and data-collection by the Rx. Collectively, these uses allow for the alignment of the Tx and Rx to a common time-base.

III. CORRELATION-BASED CHANNEL SOUNDER EXPERIMENTS

The channel sounder Tx and Rx both use an instrument backplane, into which a vector signal transceiver, a timing interface module, and a timing distribution module are installed, as shown in Fig. 1. Each of these modules, as well as the backplane, have their own quartz oscillators, which are configured to accept input from the external Rb clock. The vector signal transceiver may operate in a receive mode, where it collects 14 bit resolution in-phase and quadrature (I/Q) data at a specified frequency. It also may function as a transmitter, where 16 bit I/Q data are converted to a modulated signal at a specified frequency. We analyze the measured data to evaluate the timing offset and stability of the system.

The rubidium clock supplies a 10 MHz signal to phase-lock the channel-sounder backplane's internal quartz oscillator, and provides a 1 PPS signal to the timing input module. This signal is transmitted across the backplane and used to phase-lock the timing distribution module's internal clock. Finally, we connect the rubidium clock's 10 MHz signal directly to the vector signal transceiver. The transceiver provides a reference frequency for the transceiver's LO and digital-to-analog converter (DAC) or ADC circuits. Prior to the experiment, we verified that both the Tx and Rx rubidium clocks were set to their factory firmware presets.

In a typical channel-sounder measurement, a complex bit-sequence is modulated onto a carrier and transmitted through an over the air channel. To support the deterministic and stochastic mathematical approaches, Tx produces a sine wave at a fixed frequency of 2.25 GHz through a conducted channel using an RF coaxial cable connected between the Tx and Rx RF ports.

A. RF Signal Phase Offset and Time Offset

The received signal at the Rx is downconverted and sampled at time-points (t_i), producing a vector of in phase (I) and quadrature (Q) samples (I_i and Q_i), representing the real and imaginary RF signal components, respectively [40]. From these, we compute the relative phase offset of the RF signal as

$$\theta_i = \measuredangle(I_i + jQ_i), \tag{1}$$

$i = 0, \dots, N$, where there are $N + 1$ I/Q samples. Because the values of θ are $\theta_i \in [0, 2\pi]$, we "unwrapped" the θ values to get a continuous series of phase offsets. From these unwrapped phase offsets, we compute the timing offset, x, between the Tx and Rx by

$$x_i = \frac{\theta_i}{2\pi f_c}, \tag{2}$$

where x_i represents the measurement-derived timing offset between the Tx and Rx, in units of seconds, at time t_i. This quantity, x_i, is the basis for subsequent analysis of the components of timing offset.

IV. TIMING OFFSET ANALYSIS FOR TIMING CONFIGURATIONS

We quantify the channel sounder's timing offset ($\epsilon(t)$), using a second-order approximation of the clock behavior and noise a standard approach for characterization of oscillators [6]-[8]. Next, we analyze the properties of this noise using the stochastic mathematical approach of time deviation (TDEV) which is a time-stability form of the Allan Deviation. It is important to note that in this work, $\sigma_x(\tau)$ is calculated from x_i, not $\epsilon(t)$.

A. Timing Offset Clock Model

We quantify the timing offset of the channel sounder using a model with separate deterministic and stochastic components. Note that for our analysis, we define the Tx Rb clock as the reference clock and the Rx Rb clock as the clock under test. A second-order model for the time offset between two clocks is [7][8]:

$$x_i = x_0 + y_0 t_i + \frac{D t_i^2}{2} + \epsilon(t_i). \tag{3}$$

We describe the deterministic terms of this equation, $x_0, y_0,$ and D, in detail below. The residual term, $\epsilon(t_i)$, relates to the stochastic (noise) properties of the system. We characterize these properties using the TDEV (Section IV.B). From the TDEV, we aim to infer which noise process (Table I) are present in $\epsilon(t_i)$. Note that $\epsilon(t_i)$ can include modelling error.

The first term in (3), x_0, is known as the synchronization offset. It describes the initial deterministic time offset in seconds between the Rx Rb clock and the Tx Rb clock.

In the next term, the coefficient y_0, is known as the syntonization offset. It is a measure of the deterministic frequency offset between the Rx Rb clock and the Tx Rb clock. This timing offset is due to the imperfect knowledge of the Rb atom's hyperfine transition within each clock [42]. Nonzero values of y_0 are manifested as a time drift between the two clocks.

We define y_0 by the fractional frequency difference

$$y_0 = \frac{f_{Rx} - f_{Tx}}{f_{Tx}}, \tag{4}$$

between the Rx Rb clock frequency (f_{Rx}) and the Tx Rb clock frequency (f_{Tx}). Values of y_0 are unitless, and may be interpreted as timing drift in seconds of time drift per elapsed ddsecond. Values of y_0 may equivalently be interpreted as fractional frequency offset, as Hertz of offset per Hertz of fundamental frequency. We use the terms "time drift" and "frequency offset" interchangeably in this work, both of which refer to y_0 [44].

The third term, D, describes the deterministic frequency drift [8] [41] [43]. This term is particularly costly to estimate because it may represent the clock drift over many years. If the experimental time duration is not long enough, D cannot be estimated accurately. We present our findings of D based upon the timing configurations but we recognize a thorough analysis of this term requires long-term measurements considered outside the scope of the work presented here.

We estimate these x_0, y_0, and D with a least-squares fit of the clock-model (3) to our experimental x_i values. In Section V we quantify the deterministic timing offset between the Rb clocks in terms of x_0, y_0, and D for different timing configurations.

B. Stochastic Noise Properties, $\sigma_x(\tau)$

The last term, $\epsilon(t_i)$, in (3) describes the stochastic (noise) component of the timing offset. Whereas the exact value of $\epsilon(t_i)$ is unknown for any time t_i, we estimate the statistics of $\epsilon(t_i)$ over a finite time duration. These statistics are calculated from measurements of x_i, and are summarized by the quantity $\sigma_x(\tau)$. Such statistical analysis provides insight into the timing configurations as a suitable frequency source.

It is important to note that the variance of white noise decreases through averaging repeat measurements while other noise processes, such as a random-walk process, do not have this property. Hence, knowledge of the noise processes in the clocks is vital to understanding the channel sounder timing errors. We provide a summary of typical noise processes [8] in Table I, and example plots of computer-generated noise in Fig. 4, showing the appearance of several different types of noise.

Well-known stochastic noise analysis tools include the Allan deviation [5], the modified Allan deviation [43], and the time-deviation (TDEV) [8][44]. These tools share the general property of measuring timing stability of phase or frequency over a specified averaging time. The time interval, τ, is the time duration for TDEV computation. Since these noise analyses are not affected by the deterministic terms in (3), we can compute the noise statistics from either modeling residual or x_i. In our analysis, we used TDEV because this analysis can best discriminate between the specific types of timing noise, specifically white and flicker PM noise [8].

To compute TDEV, we first estimate the modified Allan deviation. The modified Allan deviation can distinguish between some noise types due to an additional phase averaging operation. The definition of the modified Allan deviation for discrete data is [43]:

$$\text{Mod } \sigma_y(\tau) \approx \sqrt{\frac{\sum_{j=1}^{N-3m+1} \left\{ \sum_{i=j}^{j+m-1} (x_{i+2m} - 2x_{i+m} + x_i) \right\}^2}{2(N - 3m + 1)m^4 \tau^2}} \tag{5}$$

where the averaging factor is:

$$m = \tau / \tau_0. \tag{6}$$

With τ_0 being the time interval between x_i samples. Next, we calculate the TDEV as [44]:

$$\sigma_x(\tau) = \left(\frac{\tau}{\sqrt{3}}\right) \text{Mod } \sigma_y(\tau). \qquad (7)$$

The modified Allan deviation and TDEV characterize the type of noise present in the time domain [45]. We characterized the noise of our clock timing configurations by the slope of the TDEV plots. This slope indicates the dominant noise type as a function of τ. We provide a summary of slopes, their corresponding noise processes and typical noise sources in Table I [8].

V. RESULTS AND DISCUSSION

We performed multiple acquisitions of I/Q data with a range of sampling periods and experimental durations. We derive x_i from the conducted I/Q experiments as given in Table II. Numerous experiments were performed with different combinations of experiment length and sampling rate, which allowed us to overcome a hardware limitation preventing extremely long measurements at high data rates. We estimate the timing offset quantities: x_0, y_0, D, and $\sigma_x(\tau)$ from the time offset.

We performed I/Q experiments with lengths of time relevant to channel sounding measurements, on the order of minutes to days. Henceforth, multiple-day experiments are referred to as long-term, and experiments of less than a single day are referred to as short-term.

A. Long-Term Timing Offset Results

To determine the clock effects of drift and aging for the three different timing configurations, we collected I/Q data. For each of the timing configurations, the system's I/Q was measured for at least seven days before being reconfigured for the next experiment. The x_i data for all three configurations are overlaid in Fig. 5. We performed the experiment for the untethered configuration immediately following the tethered experiment

Table I: Summary of types of noise processes, their typical sources, and the resulting slope produced on a log-log plot of $\sigma_x(\tau)$ vs. τ [8].

Slope	Noise Process Type	Typical Noise Sources
$\tau^{-\frac{1}{2}}$	White phase-modulation	Noisy electronic hardware
τ^0	Flicker phase-modulation	
$\tau^{+\frac{1}{2}}$	White frequency-modulation	Rubidium frequency-lock control loop
τ^1	Flicker frequency-modulation	Environment and low-frequency electronic hardware
$\tau^{+\frac{3}{2}}$	Random-walk frequency-modulation	Physical environmental sensitivity: temperature and mechanical shock or vibration

Table II: Sampling periods and experiment lengths.

Experiment	Sample interval (seconds per sample)	Experiment length
Short-term A	10^{-6}	100 seconds
Short-term B	0.498	249 seconds
Short-term C	1.637	816 seconds
Long-term	10	7 days

and left the PPS tether cable in place for the first 22 hours of the untethered experiment. This was done so that the effect of removing the PPS tether could be more easily observed. A black arrow illustrates this event in Fig. 5.

From Fig. 5, the common-clock line appears flat with the value of $x_i = 0$ ns. In contrast, the tethered configuration has small fluctuations near $x_i = 0$ ns. The untethered configuration has similar variations during the first 22 hours of the experiment, at which time the PPS tether was still in place. When PPS tether was disconnected, as indicated by the black
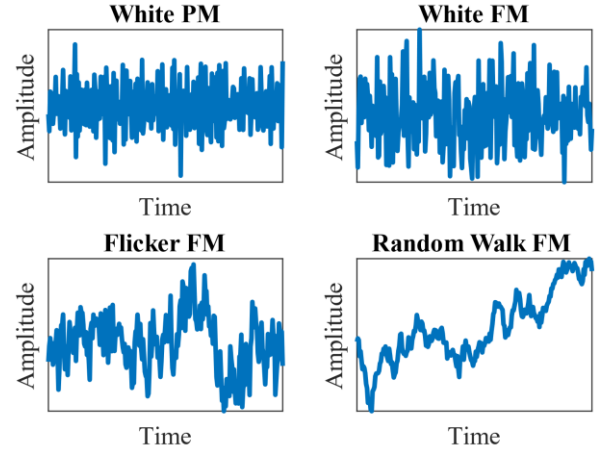
Fig. 4: Time-domain samples of four different types of simulated noise: white phase modulation (PM), white frequency modulation (FM), flicker frequency modulation, and random walk frequency modulation.
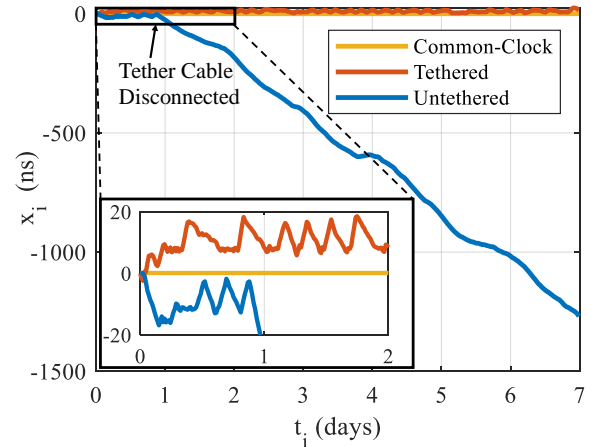
Fig. 5: Measured long-term timing drift (x_i) for the timing confgurations over multiple days. Note: in the untethered clock timing configuration, the Tx Rb clock was connected initially to the Rx clock, but they were disconnected 22 hours into the experiment.
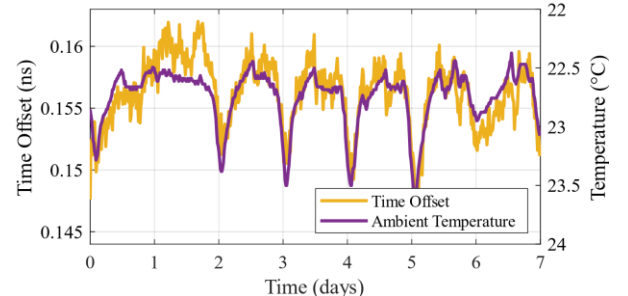
Fig. 6: Further enlarged view of Fig. 5 highlighting the single-clock timing offset with the laboratory ambient temperature overlaid (reversed temperature scale) starting after the first day of data collection.

arrow in Fig. 5, we observed a timing drift (y_0) of 2.03 ps/s as the dominant source of timing offset.

When the system was operated in the tethered configuration, small variations are seen in the timing offset, as shown in Fig. 5 (inset). These variations are the result of the control circuitry in the Rx Rb clock receiving the PPS pulses and attempting to synchronize with the Tx Rb clock.

We can see that the common-clock timing-offset variations are orders of magnitude smaller than the tethered and untethered configurations from the plot and the inset plot of Fig. 5. The timing drift of the untethered configuration was on the order of 200 ns per day, and the timing drift of the tethered configuration was near 20 ns. The residual drift of the common-clock configuration was estimated to be less than 20 ps throughout the multi-day experiment.

The second-order timing drift model (3) omits many potential effects, such as those due to temperature. We measured the ambient laboratory temperature during the single-clock experiment, as shown by the purple line of Fig. 6. A relationship appears to exist between the timing offset and the measured temperature. We did not observe similar temperature effects for the tethered and untethered configurations. This is most likely because other sources of timing noise were predominant in these configurations.

B. Short-Term Time-Offset Results

In addition to the long-term experiments, we performed a series of shorter-time-duration experiments. We chose time durations comparable to typical channel-sounding measurements: periods of minutes to hours. These short-term experiments enabled data collections at higher sampling rates and greater numbers of repeat measurements (Table II: Short-term C).

Multiple trials were conducted, where each trial comprised of 40 repeat experiments for each timing configuration. Because the dominant timing noise type corresponding to the length of these experiments appears to be flicker or random-walk (Section V.D), we cannot directly compare the results from trial to trial. We therefore selected "best-case" and "worst-case" results from our trials, where best-case had the smallest observed y_0, and worst-case had the largest average y_0. The x_0, y_0, and D results from these best-case and worst-case datasets are presented in histogram form.

1) Initial Synchronization Offset, x_0

Initial synchronization offset, x_0, is a measure of the timing offset between the Tx Rb clock and the Rx Rb clock. In the case of the short-term experiments (Table II: Short-term C), this error represents the timing offset at the start of the experiment. Since we compute x_i from the phase offset in the I/Q data, we were not able to compute x_0 outside a range of ±0.44 ns (due to the 2.25 GHz carrier frequency used) because the phase will "wrap" to a lower value outside of this range.

We present histograms of x_0 in Fig. 7 (a) and (b) for two separate trials with three timing configurations. Each subfigure contains the results of 40 repeat experiments for each timing configuration. For the common-clock configuration, the time offset was constant for all the experiments. In contrast, x_0 values for both the tethered and untethered systems are more broadly dispersed in the range of ±0.44 ns.
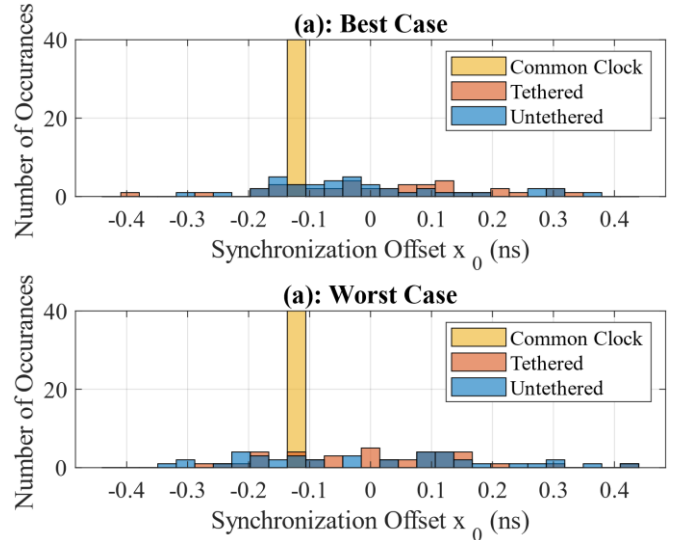
Fig. 7: Histogram of the initial synchronization offset (x_0) for (a) best-case and (b) worst-case trials.
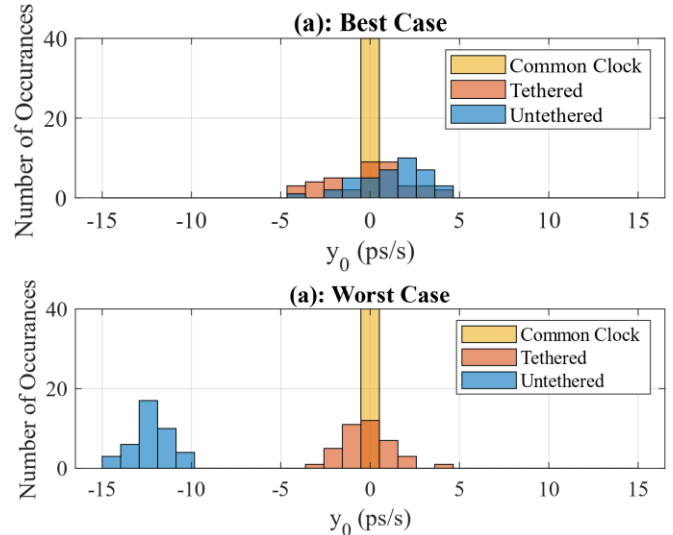
Fig. 8: Histogram of initial syntonization offset (y_0) data for 40, 100 second runs in each clock configuration for (a) best-case and (b) worst-case trials.
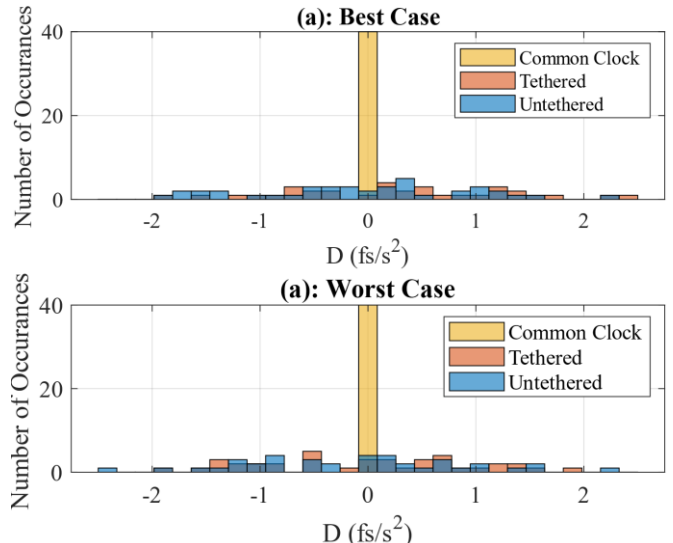
Fig. 9: Histogram of frequency drift (D) data for 40, 100 second runs in each clock configuration for (a) best-case and (b) worst-case trials.
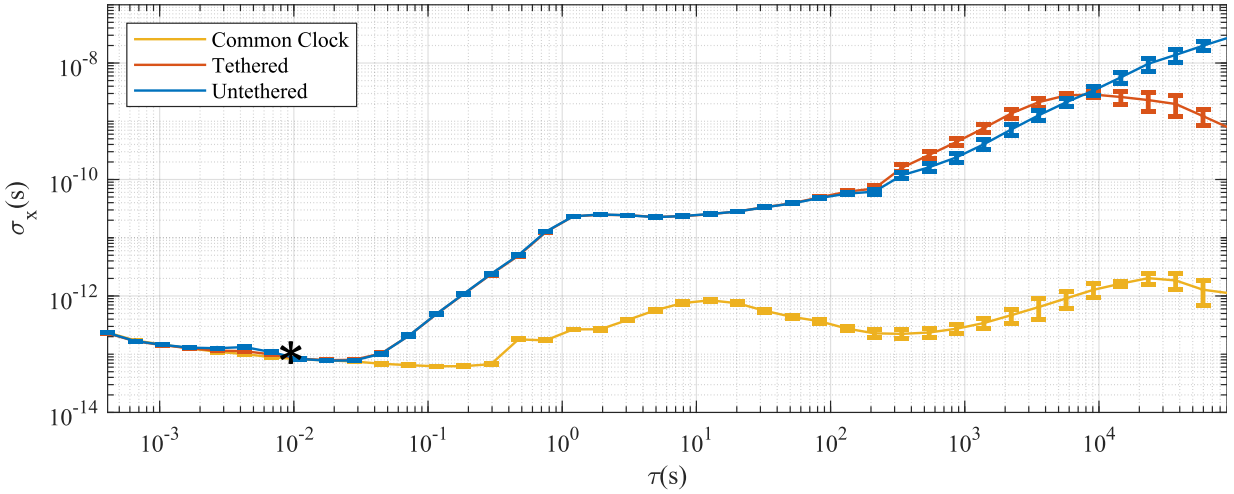
Fig. 10: Time deviation (TDEV - $\sigma_x(\tau)$) data for all experimental runs. Confidence intervals are plotted at the 99% C.I. level.

2) Syntonization Offset, y_0

Syntonization error describes the degree of time drift between the Rx Rb clock and the Tx Rb clock. This syntonization error for the timing configuration may affect a channel-sounder measurement, especially if the measurement has a long propagation path or uses millimeter-wave frequencies.

We present histogram plots in Fig. 8 (a) and (b) of the derived syntonization results (y_0) for two separate short-term (Table II Short-term C) trials with three configurations. The trial in Fig. 8 (a) is a best-case result, where the syntonization error remained very small after the PPS tether cable was disconnected. In contrast, Fig. 8 (b) represents a worst-case result, where a significant syntonization error was observed in the untethered configuration.

The data from Fig. 8 (a) are summarized in Table III, and the data from Fig. 8 (b) in Table IV. From these results, we see that y_0 had a statistically significant value only during the untethered configuration of the trial shown in Fig. 8 (b). This is consistent with other observations we made, where disconnecting the PPS cable can cause varying degrees of syntonization offset. This phenomenon is discussed further in Section V.E.

C. Frequency Drift, D

The value D is a first-order frequency drift and second-order time drift which dominates over long timescales of months or even years. We used a curve-fitting routine to estimate the frequency drift from measurements for the timing configurations with short-term experiments (Table II: Short-term C). We provide these results in Fig. 9 (a) and (b). We list approximate 95% confidence intervals [46] around the mean value of D in Table V. These intervals are based around the assumption of independent Gaussian measurement noise and so should be interpreted only as a summary of the data. Note that each of these approximate intervals contains zero. This reflects the difficulty in estimating D over short time scales due to the predominance of timing noise and first-order timing drift in short-term experiments. Nonetheless, we provide this information for completeness and to be consistent with the clock model (3).

D. Stochastic (Noise) Component TDEV Results, σ_x

By applying the deterministic clock model (3) to our measured timing offset data, we illustrate that the data have certain statistically significant, deterministic properties. In order to understand the stochastic properties of our timing offset data, the TDEV (7) was applied to all of the datasets listed in Table II, both short-term and long-term. We computed the mean values for TDEV from all datasets, and their confidence intervals at the 99% level [46] and plotted these results in Fig. 10.

Values of TDEV are plotted with $\sigma_x(\tau)$ as a function of τ. A log-log scale is used to provide a compact representation for the large range of values within the plot. Due to this log-log scale, the exponential slopes listed in Table I appear as linear slopes on our plot. By examining the slope of $\sigma_x(\tau)$ values near a given value of τ, a qualitative analysis may be made as to the type of noise present at that averaging time. A limitation of the TDEV method is that the uncertainty of $\sigma_x(\tau)$ increases as τ approaches the total experiment length. We truncate our results at 9×10^4 s for this reason.

Table III: Mean ($\bar{y}_0$) and standard deviation ($S_{DEV}(y_0)$) for the syntonization offset (y_0) corresponding to Fig. 8(a).

	$\bar{y}_0$	$S_{DEV}(y_0)$
Single Clock	1.3×10^{-17}	1.0×10^{-15}
Two Clocks: Tethered	-5.5×10^{-14}	2.2×10^{-12}
Two Clocks: Untethered	1.2×10^{-12}	1.9×10^{-12}

Table IV: Mean ($\bar{y}_0$) and standard deviation ($S_{DEV}(y_0)$) for the syntonization offset (y_0) corresponding to Fig. 8(b).

	$\bar{y}_0$	$S_{DEV}(y_0)$
Single Clock	-8.3×10^{-16}	7.3×10^{-15}
Two Clocks: Tethered	-1.4×10^{-13}	1.4×10^{-12}
Two Clocks: Untethered	-1.2×10^{-11}	1.1×10^{-12}

Table V: Mean values and confidence intervals (95%) around values of frequency drift (D) corresponding to Fig. 9.

	Best Case	Worst Case
Single Clock	3.3×10^{-19} $\pm\ 2.3 \times 10^{-18}$	1.8×10^{-20} $\pm\ 3.1 \times 10^{-19}$
Two Clocks: Tethered	4.7×10^{-17} $\pm\ 3.4 \times 10^{-16}$	2.1×10^{-16} $\pm\ 5.8 \times 10^{-16}$
Two Clocks: Untethered	-6.5×10^{-17} $\pm\ 3.6 \times 10^{-16}$	-5.0×10^{-17} $\pm\ 3.2 \times 10^{-16}$

In the left portion of Fig. 10, we observe that for all timing configurations, $\sigma_x(\tau)$ have similar slopes and magnitudes for τ less than 10^{-2} seconds (denoted by a star on the plot). At these τ values, σ_x is dominated by white phase-modulation (PM) and flicker PM noises. From this information, we can understand that the channel sounder's electronic hardware is the dominant noise source at this averaging time, for all timing configurations from Table I. Potential noisy electronic hardware sources may be channel sounder internal timing configuration, low noise amplifiers, or mixers.

For τ between 10^{-2} and 10^3 seconds, the common-clock configuration TDEV diverges from the tethered and untethered configurations. From this result, we infer that the dominant noise process depends upon the timing configuration for longer periods of time. The common-clock noise process is either white PM or flicker PM. Over the same time period, the tethered and untethered timing configurations exhibit a flicker frequency-modulation (FM) process. Flicker FM often results from low-frequency electronics and physical environmental effects such as temperature. The fact that both the tethered and untethered systems exhibit similar levels of noise in this region implies that this noise comes from the clocks themselves, and not the synchronization circuitry.

At τ greater than 10^3 seconds, the untethered timing configuration exhibits a flicker or random-walk noise process, while the tethered timing configuration has a stationary Gaussian-type noise process. This Gaussian noise may be indicative of the time-synchronization circuitry limiting the maximum time deviation between the clocks. This is in contrast to the untethered configuration, which exibits a continued random-walk noise due to a lack of syntonization.

Thus, the use of TDEV provides us a qualitative tool to understand the timing noise in our channel sounder. These results become particularly meaningful when different timing or clock configurations are compared. From Fig. 10, a strong contrast may be observed between the TDEV results for common-clock and tethered or untethered.

E. Determination of Clock Synchronization for the Untethered Configuration

The measurements presented in the previous sections of this work provide insight into separate timing configurations of the channel sounder. In a typical channel-sounding campaign, these configurations are not used in isolation. Rather, the system is assembled (if taken apart for shipping) and powered-on in an unsynchronized (cold-start) state. Then, the system is placed into the tethered configuration and allowed to synchronize. Finally, the Tx and Rx are disconnected, and channel measurements are carried out.

To gain insight into this process, we performed these steps on our correlation-based channel sounder, beginning with a cold-start state where the clocks, Tx, and Rx were powered off. In the case of our system, we found that the synchronization process took approximately 12 hours, and once the clocks were untethered, they immediately demonstrated a frequency-offset within the manufacturer's "settability" specification of 5×10^{-12} seconds per second, or 432 ns per day [40].

For our first set of timing offset experiments for the untethered configuration, we simulated the "cold-start" step by removing the power to the Tx and Rx Rb clocks, waiting five minutes, and then returning the power to the clocks. Next, we began measuring the I/Q data to determine the initial state of the clocks. We repeated the experiment for three trials. Note: we did not synchronize the clocks using the PPS coaxial cable during these trials.

We show the timing offset from these trials in Fig. 11. In all three trials, we observed a time drift of approximately 40 μs per day. This offset is significantly greater than the 200 ns per day from Fig. 5. Whereas in Fig. 5 the clocks had recently been synchronized prior to the experiment, the clocks in Fig. 11 are in a cold-start state, and have not been synchronized since powering on.

The next set of untethered configuration experiments we ran were to determine the amount of time required to return to the synchronization of a tethered configuration after being in an untethered configuration. Between these two configurations, the tethered configuration is the preferred configuration since it
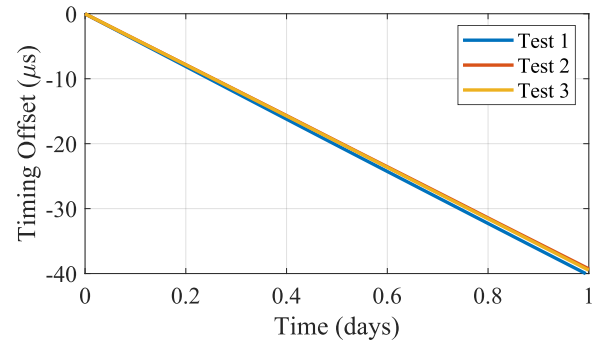
Fig. 11: Time offset data collected from rubidium clocks which were newly powered on, without synchronization.
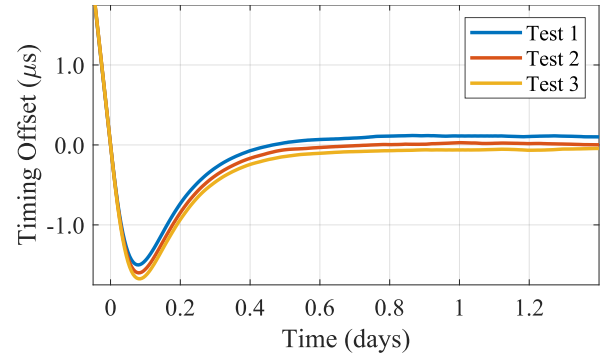
Fig. 12: Previously unsynchronized rubidium clocks, connected by PPS synchronization cable at the time indicated by the yellow diamond.
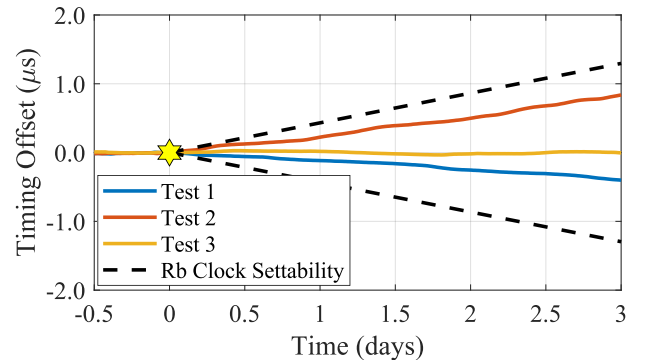
Fig. 13: Clocks after 48 hours of synchronization, with the PPS synchronization cable disconnected at the time indicated by the black star. Dashed black lines indicate the manufacturer specified "settability" of the clocks: 5×10^{-12} seconds per second, or 432 ns/day [40].

had less timing offset over a multi-day experiment. To determine this time, we analyze the timing offset as given in Fig. 12. We can see the effects of reconnecting the Tx and Rx Rb clocks together using the PPS coaxial cable indicated by a diamond symbol. Prior to the reconnection of the PPS coaxial cable, the mean time drift was 39.7 microseconds per day, as shown in Fig. 11. Once the Tx and Rx Rb clocks are connected using the PPS coaxial cable (indicated after the diamond symbol), we observed that the timing offset takes up to 24 hours to stabilize.

In the last set of experiments, we disconnected the PPS coaxial cable to quantify the timing offset associated with the disconnection of the Tx and Rx Rb clocks for an untethered configuration. In each experiment, we first connected the Tx and Rx Rb clocks using the PPS coaxial cable for up to 48 hours. We then measured the I/Q data for calculation of the timing offset, as seen in Fig. 13. Once again, we can see the effects of the PPS coaxial cable disconnection as depicted by the star (*) symbol in Fig. 13. We observed that a change in the timing offset occurs immediately after the PPS tether was disconnected. The rate and direction of time drift was variable between the experimental sets, even when we used the same hardware and channel sounder configuration (i.e., sampling rate). All observed time drifts fell within the clock manufacturer's reported "settability" bound [40], which describes the "worst-case" attainable synchronization accuracy.

We find that synchronization utilizing a PPS coaxial cable is effective at reducing drift from the high level seen with newly powered-on clocks, to a level that lies within the manufacturer's settability specification (Fig. 13).

One important observation from these channel-sounder operational experiments is that clocks undergo cycles of timing offset when in the tethered configuration, as illustrated in Fig. 4. These oscillations are likely a product of the control circuitry in the Rx Rb clock, which receives the PPS pulses, attempts to track the phase of the Tx Rb clock. A secondary observation is the unpredictable behavior of the clocks after the PPS coaxial cable was disconnected from the Tx and Rx Rb clocks, as shown in Fig. 13. However, all the measured time drifts fall within the settability bounds provided by the manufacturer.

The measurements presented in this section comprise a simple diagnostic procedure by which the quality of time synchronization and the degree of timing drift may be characterized for systems of two-clocks. The results presented are applicable to the specific pair of clocks used in our experiments, but the measurement and analytic approaches are still applicable. Regarding channel sounding, these measurements comprise a practical check on a system's timing.

VI. CONCLUSIONS

Channel sounders are commonly constructed with a Rb clock in both the Tx and Rx, which enables time synchronization and syntonization without a physical cable between the Tx and Rx, untethered clock configuration. To understand the limitations of such a configuration, we studied a functioning 1-6 GHz channel sounder which incorporates a pair of Rb clocks. We compared the untethered timing configuration to a tethered configuration, where the Rx is synchronized to the Tx by phase-locking to a 1 PPS signal carried by a coaxial cable.

Additionally, we compared a third clock configuration known as a common-clock configuration, where both the Tx and Rx were referenced to one Rb clock.

Using a second-order clock model for timing offset, we observed that the time drift differs each time the PPS coaxial cable is disconnected. Upon re-connecting this cable, we see that the Rx clock takes up to 12 hours to synchronize with the Tx clock. Through this timing synchronization, we achieved timing offset and drift within the manufacturer's specifications for the Rb clock. As part of our best measurement practices, we have determined to connect the Tx and Rx clocks for at least 12 hours prior to any measurement campaign. We note that the time required for synchronization is dependent on the specific clock hardware: changes in the clock hardware would require re-evaluation.

We additionally observed and characterized the timing noise in the separate clock configurations. The dominant noise process was directly dependent upon the clock configuration. We noted the presence of a flicker FM noise in the tethered and untethered configurations. The presence of this noise component is significant because standard deviation of channel measurements impacted by this non-stationary process does not necessarily decrease with averaging multiple measurements. The relationship between timing offset, timing noise, and the uncertainty of measured signals is a subject for future research in our channel sounding uncertainty analysis.

High-quality data-driven models require an understanding of the frequency standard imperfections. In this work, we provide a method to quantify the timing offset and timing noise of a correlation-based channel sounder. This method can extend to any system with a dual-clock configuration. Timing offset and noise are known to impact numerous types of modulated signals. The exact relationship between timing offset and uncertainty of measured signals is a subject for future research.

VII. REFERENCES

[1] A. Zaidi, F. Athley, J. Medbo, U. Gustavsson, G. Durisi, and X. Chen, *5G Physical Layer: Principles, Models and Technology Components*. Orlando, FL, US: Academic Press, 2018.

[2] J. T. Quimby *et al.*, "NIST channel sounder overview and channel measurements in manufacturing facilities," National Institute of Standards and Technology, Gaithersburg, MD, NIST TN 1979, Nov. 2017. https://doi.org/10.6028/NIST.TN.1979

[3] J. M. Kast, "Quantification of Timing Uncertainty in a Correlation Based Channel Sounder," Master's thesis, Colorado School of Mines, Golden, USA, November 2018.

[4] G. R. MacCartney and T. S. Rappaport, "A Flexible Millimeter-Wave Channel Sounder With Absolute Timing," in *IEEE Journal on Selected Areas in Communications*, vol. 35, no. 6, pp. 1402-1418, June 2017, doi: 10.1109/JSAC.2017.2687838.

[5] D. W. Allan, "Statistics of atomic frequency standards," in *Proceedings of the IEEE*, vol. 54, no. 2, pp. 221-230, Feb. 1966, doi: 10.1109/PROC.1966.4634.

[6] J. A. Barnes, "Atomic timekeeping and the statistics of precision signal generators," in *Proceedings of the IEEE*, vol. 54, no. 2, pp. 207-220, Feb. 1966, doi: 10.1109/PROC.1966.4633.

[7] D. W. Allan, "Time and Frequency (Time-Domain) Characterization, Estimation, and Prediction of Precision Clocks and Oscillators," in *IEEE Transactions on Ultrasonics, Ferroelectrics, and Frequency Control*, vol. 34, no. 6, pp. 647-654, Nov. 1987, doi: 10.1109/T-UFFC.1987.26997.

[8] W. J. Riley, "Handbook of frequency stability analysis," National Institute of Standards and Technology, Gaithersburg, MD, NIST Special Publication 1065, 2008.

[9] J. Lee, J. Liang, J. Park and M. Kim, "Directional path loss characteristics of large indoor environments with 28 GHz measurements," *2015 IEEE*

26th Annual International Symposium on Personal, Indoor, and Mobile Radio Communications (PIMRC), Hong Kong, China, 2015, pp. 2204-2208, doi: 10.1109/PIMRC.2015.7343663.

[10] H. Kwon, M. Kim and Y. Chong, "Implementation and performance evaluation of mmWave channel sounding system," *2015 IEEE International Symposium on Antennas and Propagation & USNC/URSI National Radio Science Meeting*, Vancouver, BC, Canada, 2015, pp. 1011-1012, doi: 10.1109/APS.2015.7304893.

[11] R. J. Weiler, M. Peter, T. Kühne, M. Wisotzki and W. Keusgen, "Simultaneous millimeter-wave multi-band channel sounding in an urban access scenario," *2015 9th European Conference on Antennas and Propagation (EuCAP)*, Lisbon, 2015, pp. 1-5.

[12] S. Li, Y. Liu, Z. Chen, X. Sun and L. Lin, "Measurements and modelling of millimeter-wave channel at 28 GHz in the indoor complex environment for 5G radio systems," *2017 9th International Conference on Wireless Communications and Signal Processing (WCSP)*, Nanjing, 2017, pp. 1-6.

[13] R. S. Thomä, D. Hampicke, A. Richter, G. Sommerkorn, and U. Trautwein, "MIMO vector channel sounder measurement for smart antenna system evaluation," *European Transactions on Telecommunications*, vol. 12, no. 5, pp. 427–438, 2001.

[14] G. R. MacCartney, H. Yan, S. Sun and T. S. Rappaport, "A flexible wideband millimeter-wave channel sounder with local area and NLOS to LOS transition measurements," *2017 IEEE International Conference on Communications (ICC)*, Paris, France, 2017, pp. 1-7, doi: 10.1109/ICC.2017.7996791.

[15] D. R. Novotny, A. E. Curtin, K. A. Remley, P. B. Papazian, J. T. Quimby, and R. Candell. "A tetherless, absolute-time channel sounder, processing, and results for a complex environment," 2016 *Proceedings of the Antenna Measurement Techniques Association*, Austin, TX, United States.

[16] D. Caudill, P. B. Papazian, C. Gentile, J. Chuang and N. Golmie, "Omnidirectional Channel Sounder With Phased-ArrayAntennas for 5G Mobile Communications," in *IEEE Transactions on Microwave Theory and Techniques*, vol. 67, no. 7, pp. 2936-2945, July 2019, doi: 10.1109/TMTT.2019.2910109.

[17] R. Zhang, S. Wang, X. Lu, W. Duan and L. Cai, "Two-Dimensional DoA Estimation for Multipath Propagation Characterization Using the Array Response of PN-Sequences," in *IEEE Transactions on Wireless Communications*, vol. 15, no. 1, pp. 341-356, Jan. 2016, doi: 10.1109/TWC.2015.2473156.

[18] Z. Wen *et al.*, "mmWave channel sounder based on COTS instruments for 5G and indoor channel measurement," *2016 IEEE Wireless Communications and Networking Conference*, Doha, Qatar, 2016, pp. 1-7, doi: 10.1109/WCNC.2016.7564643.

[19] J. Li, P. Zhang, C. Yu, H. Wang and W. Hong, "High-Efficiency Wideband Millimeter-Wave Channel Sounder System," *2019 13th European Conference on Antennas and Propagation (EuCAP)*, Krakow, Poland, 2019, pp. 1-5.

[20] C. U. Bas *et al.*, "A Real-Time Millimeter-Wave Phased Array MIMO Channel Sounder," *2017 IEEE 86th Vehicular Technology Conference (VTC-Fall)*, Toronto, ON, Canada, 2017, pp. 1-6, doi: 10.1109/VTCFall.2017.8287875.

[21] C. U. Bas *et al.*, "Real-Time Millimeter-Wave MIMO Channel Sounder for Dynamic Directional Measurements," in *IEEE Transactions on Vehicular Technology*, vol. 68, no. 9, pp. 8775-8789, Sept. 2019, doi: 10.1109/TVT.2019.2928341.

[22] S. Salous, S. M. Feeney, X. Raimundo and A. A. Cheema, "Wideband MIMO Channel Sounder for Radio Measurements in the 60 GHz Band," in IEEE Transactions on Wireless Communications, vol. 15, no. 4, pp. 2825-2832, April 2016, doi: 10.1109/TWC.2015.2511006.

[23] S. Salous, "Multi-band multi-antenna chirp channel sounder for frequencies above 6 GHz," *2016 10th European Conference on Antennas and Propagation (EuCAP)*, Davos, Switzerland, 2016, pp. 1-4, doi: 10.1109/EuCAP.2016.7481753.

[24] B. Montenegro-Villacieros, S. Salous, J. Bishop and X. Raimundo, "Channel propagation experimental measurements and simulations at 52 GHz", 32nd URS GASS, Montreal, August 2017.

[25] T. Zhou, C. Tao, S. Salous, L. Liu and Z. Tan, "Implementation of an LTE-Based Channel Measurement Method for High-Speed Railway Scenarios," in *IEEE Transactions on Instrumentation and Measurement*, vol. 65, no. 1, pp. 25-36, Jan. 2016, doi: 10.1109/TIM.2015.2477166.

[26] P. Paschalidis, M. Wisotzki, A. Kortke, W. Keusgen and M. Peter, "A Wideband Channel Sounder for Car-to-Car Radio Channel Measurements at 5.7 GHz and Results for an Urban Scenario," *2008 IEEE 68th Vehicular Technology Conference*, Calgary, BC, 2008, pp. 1-5.

[27] F. Erden, O. Ozdemir, W. Khawaja and I. Guvenc, "Correction of Channel Sounding Clock Drift and Antenna Rotation Effects for mmWave Angular Profile Measurements," in *IEEE Open Journal of Antennas and Propagation*, vol. 1, pp. 71-87, 2020, doi: 10.1109/OJAP.2020.2979243.

[28] R. Sun and P. B. Papazian, "Time Stability of Untethered Electronic Switched MIMO Millimeter-Wave Channel Sounders," in *IEEE Access*, vol. 8, pp. 21052-21062, 2020

[29] B. T. Maharaj, L. P. Linde, J. W. Wallace and M. Jensen, "A cost-effective wideband MIMO channel sounder and initial co-located 2.4 GHz and 5.2 GHz measurements," *Proceedings. (ICASSP '05). IEEE International Conference on Acoustics, Speech, and Signal Processing, 2005.*, Philadelphia, PA, USA, 2005, pp. iii/981-iii/984 Vol. 3, doi: 10.1109/ICASSP.2005.1415876.

[30] B. T. Maharaj, J. W. Wallace, M. A. Jensen and L. P. Linde, "A Low-Cost Open-Hardware Wideband Multiple-Input–Multiple-Output (MIMO) Wireless Channel Sounder," in *IEEE Transactions on Instrumentation and Measurement*, vol. 57, no. 10, pp. 2283-2289, Oct. 2008, doi: 10.1109/TIM.2008.919943.

[31] J. W. Wallace, "BYU wideband MIMO channel sounder technical reference manual." (2007).

[32] M. Kim, J.-I. Takada, and K. Saito, ''Multi-dimensional radio channel measurement, analysis and modeling for high frequency bands,'' *IEICE Trans. Commun.,* vol. E101.B, no. 2, pp. 293–308, 2018.

[33] M. Kim, Y. Konishi, Y. Chang and J. Takada, "Large Scale Parameters and Double-Directional Characterization of Indoor Wideband Radio Multipath Channels at 11 GHz," in *IEEE Transactions on Antennas and Propagation*, vol. 62, no. 1, pp. 430-441, Jan. 2014, doi: 10.1109/TAP.2013.2288633.

[34] Y. Konishi, Y. Chang, M. Kim and J. Takada, "Versatile radio channel sounder for double directional and multi-link MIMO channel measurements at 11 GHz." *IEICE Transactions on Electronics* 97.10 (2014): 994-1004

[35] G. Crotti, A. D. Femine, D. Gallo, D. Giordano, C. Landi and M. Luiso, "Measurement of the Absolute Phase Error of Digitizers," in *IEEE Transactions on Instrumentation and Measurement*, vol. 68, no. 6, pp. 1724-1731, June 2019, doi: 10.1109/TIM.2018.2888919

[36] C. Andrich, A. Ihlow, J. Bauer, N. Beuster and G. Del Galdo, "High-Precision Measurement of Sine and Pulse Reference Signals Using Software-Defined Radio," in *IEEE Transactions on Instrumentation and Measurement*, vol. 67, no. 5, pp. 1132-1141, May 2018, doi: 10.1109/TIM.2018.2794940.

[37] M. Siccardi, D. Rovera and S. Romisch, "Delay measurements of PPS signals in timing systems," *2016 IEEE International Frequency Control Symposium (IFCS)*, New Orleans, LA, 2016, pp. 1-6, doi: 10.1109/FCS.2016.7563588.

[38] J. Levine, "Invited Review Article: The statistical modeling of atomic clocks and the design of time scales," *Rev. Sci. Instrum.*, vol. 83, no. 2, Feb. 2012.

[39] "FS725 Rubidium Frequency Standard Operation and Service Manual." Stanford Research Systems, 21-Dec-2015.

[40] L. W. Couch, *Digital and analog communication systems*. New York, NY, USA: Macmillan, 1987.

[41] D. B. Sullivan, D. W. Allan, D. A. Howe, and F. L. Walls. "Characterization of Clocks and Oscillators." National Institute of Standards and Technology, Gaithersburg, MD, NIST Technical Note 1337, 1990.

[42] D. W. Allan and J. A. Barnes, "A Modified 'Allan Variance' with Increased Oscillator Characterization Ability," in *Thirty Fifth Annual Frequency Control Symposium*, 1981, pp. 470–475.

[43] D. W. Allan, D. D. Davis, J. Levine, M. A. Weiss, N. Hironaka, and D. Okayama, "New inexpensive frequency calibration service from NIST," in *44th Annual Symposium on Frequency Control*, 1990, pp. 107–116.

[44] P. Lesage and T. Ayi, "Characterization of Frequency Stability: Analysis of the Modified Allan Variance and Properties of Its Estimate," *IEEE Trans. Instrum. Meas.*, vol. 33, no. 4, pp. 332–336, 1984.

[45] L. L. Lewis, "An introduction to frequency standards," *Proc. IEEE*, vol. 79, no. 7, pp. 927–935, Jul. 1991.

[46] G. W. Snedecor and W. G. Cochran *Statistical Methods*. 8th ed. Ames, IA, USA: Iowa State University Press, 1989.